Chemistry of Polynuclear Metal Complexes with Bridging Carbene or Carbyne Ligands. Part 87.[1] Docosahedral Carbaborane(alkylidyne)tungsten Complexes as Reagents for the Synthesis of Compounds with Heteronuclear Metal–Metal Bonds: Crystal Structures of $[NEt_4][W(\equiv CC_6H_3Me_2\text{-}2,6)(CO)_2(\eta^6\text{-}C_2B_{10}H_{10}Me_2)]$ and $[NEt_4][WFe(\mu\text{-}CC_6H_3Me_2\text{-}2,6)(CO)_4(\eta^6\text{-}C_2B_{10}H_{10}Me_2)]$ *

Susan J. Crennell, David D. Devore, Sandra J. B. Henderson, Judith A. K. Howard, and F. Gordon A. Stone
Department of Inorganic Chemistry, The University, Bristol BS8 1TS

Addition of thf (tetrahydrofuran) solutions of the salt $Na_2[C_2B_{10}H_{10}Me_2]$ to thf solutions of the compounds $[W(\equiv CR)Cl(CO)_2L_2]$ (R = C_6H_4Me-4 or $C_6H_3Me_2$-2,6; L = pyridine or 4-methylpyridine), in the presence of $[NEt_4]Cl$, affords the complexes $[NEt_4][W(\equiv CR)(CO)_2(\eta^6\text{-}C_2B_{10}H_{10}Me_2)]$ in good yield. An *X*-ray diffraction study on the product with R = $C_6H_3Me_2$-2,6 reveals that the tungsten atom is ligated by two CO groups, the alkylidyne fragment [W≡C 1.84(1) Å], and the carbaborane cage. The open face of the latter is η^6-co-ordinated to the tungsten but is decidedly non-planar. The requirement of a six-atom BCBBBC ring above a pentagonal belt of five boron atoms results in two faces in the cage distorting from a triangular to an essentially square arrangement. Variable-temperature n.m.r. studies showed that in solution the anions undergo a dynamic exchange process. Treatment of the salts $[NEt_4][W(\equiv CR)(CO)_2(\eta^6\text{-}C_2B_{10}H_{10}Me_2)]$ with the reagents $[AuCl(PPh_3)]$ and $[Rh(cod)(PPh_3)_2][PF_6]$ (cod = cyclo-octa-1,5-diene) yields the dimetal compounds $[WAu(\mu\text{-}CR)(CO)_2(PPh_3)(\eta^6\text{-}C_2B_{10}H_{10}Me_2)]$ and $[WRh(\mu\text{-}CR)(CO)_2(PPh_3)_2(\eta^6\text{-}C_2B_{10}H_{10}Me_2)]$, respectively. The tungsten–gold species, and the compound $[WRh(\mu\text{-}CC_6H_4Me\text{-}4)(CO)_2(PPh_3)_2(\eta^6\text{-}C_2B_{10}H_{10}Me_2)]$, are formed as mixtures of two isomers. The reaction between $[NEt_4][W(\equiv CC_6H_4Me\text{-}4)(CO)_2(\eta^6\text{-}C_2B_{10}H_{10}Me_2)]$ and $[Fe_2(CO)_9]$ affords the trimetallic complex $[NEt_4][WFe_2(\mu_3\text{-}CC_6H_4Me\text{-}4)(\mu\text{-}\sigma\text{:}\sigma'\text{:}\eta^6\text{-}C_2B_{10}H_8Me_2)(CO)_8]$. In the latter, the carbaborane fragment has slipped over the WFe_2 triangle so that two boron atoms in the face of the cage form σ bonds with the iron atoms. The *p*-tolylmethylidyne group caps the other side of the metal triangle. In contrast, the reaction between the compounds $[NEt_4][W(\equiv CC_6H_3Me_2\text{-}2,6)(CO)_2(\eta^6\text{-}C_2B_{10}H_{10}Me_2)]$ and $[Fe_2(CO)_9]$ in thf gives the novel bimetallic complex $[NEt_4][WFe(\mu\text{-}CC_6H_3Me_2\text{-}2,6)(CO)_4(\eta^6\text{-}C_2B_{10}H_{10}Me_2)]$, the structure of which has been established by an *X*-ray diffraction study. In the anion a very short W–Fe bond [2.512(2) Å] is bridged by the xylylmethylidyne ligand [μ-C–W 2.02(1), μ-C–Fe 1.82(1) Å]. Both metal centres carry two terminally bound CO groups. As expected, the tungsten atom is ligated by the six atoms in the open face of the carbaborane cage, but the latter also bridges the W–Fe linkage *via* an exopolyhedral B–H→Fe three-centre two-electron bond. The n.m.r. data (^1H, $^{13}C\text{-}\{^1H\}$, $^{11}B\text{-}\{^1H\}$, and $^{31}P\text{-}\{^1H\}$) for the new compounds are reported, and where appropriate are discussed.

In a series of recent papers[1,2] we have demonstrated that salts of the anionic complexes $[W(\equiv CR)(CO)_2(\eta^5\text{-}C_2B_9H_9Me_2)]^-$ (R = alkyl or aryl) and $[Mo(\equiv CC_6H_4Me\text{-}4)(CO)\{P(OMe)_3\}(\eta^5\text{-}C_2B_9H_9Me_2)]^-$ can be used as precursors for the synthesis of a variety of compounds with heteronuclear metal–metal bonds. In reactions of these anionic species the C≡M (M = W or Mo) groups ligate low-valent metal–ligand fragments, thereby forming products having core structures based on a dimetallacyclopropene ring.[3] However, an intriguing aspect of this synthetic procedure is the regularity with which the *nido*-icosahedral $\eta^5\text{-}C_2B_9H_9Me_2$ fragment, bonded to the tungsten or molybdenum centres, adopts a non-spectator role. Initially this takes the form of cage slippage so as to form an exopolyhedral B–H→metal bond. However, further transformations often follow, promoted either by migration of the agostic hydrogen to the alkylidyne group or by loss of molecular hydrogen. As a result, several novel compounds have been characterised with molecular structures of a hitherto unknown type.

In this paper we introduce a new but related series of reactions based on using the salts $[NEt_4][W(\equiv CR)(CO)_2(\eta^6\text{-}C_2B_{10}H_{10}Me_2)]$ [R = C_6H_4Me-4 (**1a**) or $C_6H_3Me_2$-2,6 (**1b**)] as reagents for preparing polynuclear metal compounds. These salts contain the thirteen-vertex docosahedral $C_2B_{10}W$ framework, rather than the twelve-vertex icosahedral C_2B_9W group involved in earlier work.[2] It was anticipated that the new reagents (**1**) would display reactivity patterns different from those discovered earlier. As yet little is known about the ligand properties of the $\eta^6\text{-}C_2B_{10}H_{10}Me_2$ group, whereas those of the $\eta^5\text{-}C_2B_9H_9Me_2$ moiety are well documented. The possibility of preparing the salts (**1**) stemmed from the work of Hawthorne and co-workers[4] who showed that the *nido*-anions $[C_2B_{10}H_{10}R'_2]^{2-}$ (R′ = H or Me) could be generated *in situ* from $C_2B_{10}H_{10}R'_2$ by employing sodium dihydronaphthylide as the reducing agent. A preliminary account has been given of the results described in this paper.[5]

* *Supplementary data available:* see Instructions for Authors, *J. Chem. Soc., Dalton Trans.*, 1989, Issue 1, pp. xvii—xx.

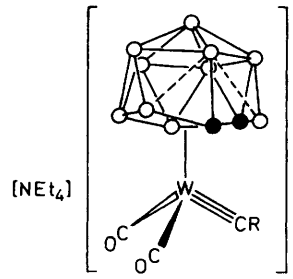

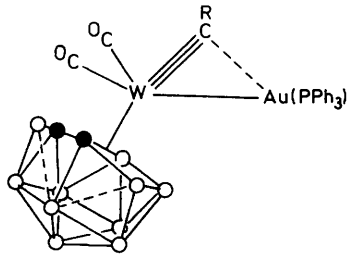

○ BH ● CMe

	R
(1a)	C_6H_4Me-4
(1b)	$C_6H_3Me_2$-2,6

	R
(2a)	C_6H_4Me-4
(2b)	$C_6H_3Me_2$-2,6

Table 1. Analytical[a] and physical data for the complexes

Compound	Yield (%)	Colour	$\nu_{max.}$(CO)[b]/cm^{-1}	Analysis (%) C	H	N
(**1a**) $[NEt_4][W(\equiv CC_6H_4Me\text{-}4)(CO)_2(\eta^6\text{-}C_2B_{10}H_{10}Me_2)]$	72	Yellow	1 990vs, 1 930s	41.1 (40.9)	6.9 (6.7)	2.2 (2.2)
(**1b**) $[NEt_4][W(\equiv CC_6H_3Me_2\text{-}2,6)(CO)_2(\eta^6\text{-}C_2B_{10}H_{10}Me_2)]$	71	Yellow	1 989vs, 1 930s	41.9 (41.9)	6.9 (6.9)	2.4 (2.1)
(**2a**) $[WAu(\mu\text{-}CC_6H_4Me\text{-}4)(CO)_2(PPh_3)(\eta^6\text{-}C_2B_{10}H_{10}Me_2)]$	82	Yellow	[c]2 028s, 1 981s	38.7 (39.4)	4.2 (3.9)	
(**2b**) $[WAu(\mu\text{-}CC_6H_3Me_2\text{-}2,6)(CO)_2(PPh_3)(\eta^6\text{-}C_2B_{10}H_{10}Me_2)]$	56	Yellow	2 034s, 1 986s	[d]40.9 (41.3)	4.4 (4.4)	
(**3a**) $[WRh(\mu\text{-}CC_6H_4Me\text{-}4)(CO)_2(PPh_3)_2(\eta^6\text{-}C_2B_{10}H_{10}Me_2)]$	84	Brown	[c,e]2 001s, 1 987 (sh), 1 962s, 1 808m	53.1 (52.6)	4.9 (4.7)	
(**3b**) $[WRh(\mu\text{-}CC_6H_3Me_2\text{-}2,6)(CO)_2(PPh_3)_2(\eta^6\text{-}C_2B_{10}H_{10}Me_2)]$	81	Dark green	2 010s, 1 787m	52.4 (53.0)	4.9 (4.8)	
(**4**) $[NEt_4][WFe_2(\mu_3\text{-}CC_6H_4Me\text{-}4)(\mu\text{-}\sigma\text{:}\sigma'\text{:}\eta^6\text{-}C_2B_{10}H_8Me_2)(CO)_8]$	70	Dark green	2 034m, 1 990vs (br), 1 962m, 1 950 (sh), 1 938 (sh)	36.7 (36.4)	4.5 (4.5)	1.6 (1.5)
(**5**) $[NEt_4][WFe(\mu\text{-}CC_6H_3Me_2\text{-}2,6)(CO)_4(\eta^6\text{-}C_2B_{10}H_{10}Me_2)]$	41	Green	2 002m, 1 950vs, 1 900m	39.0 (38.9)	6.1 (5.9)	2.0 (1.8)

[a] Calculated values are given in parentheses. [b] In CH_2Cl_2, unless otherwise stated. A broad band due to ν(B–H) is observed in the range 2 523 to 2 554 cm^{-1}. [c] In thf. [d] Recrystallised from acetone; analysis includes one molecule of solvent. [e] Two isomers (see text).

Results and Discussion

Treatment of thf (tetrahydrofuran) solutions of $[W(\equiv CR)Cl(CO)_2L_2]$ (R = C_6H_4Me-4 or $C_6H_3Me_2$-2,6; L = pyridine or 4-methylpyridine) with $Na_2[C_2B_{10}H_{10}Me_2]$, in the presence of $[NEt_4]Cl$, gives the salts $[NEt_4][W(\equiv CR)(CO)_2(\eta^6\text{-}C_2B_{10}H_{10}Me_2)]$ [R = C_6H_4Me-4 (**1a**) or $C_6H_3Me_2$-2,6 (**1b**)], characterised by microanalysis and by spectroscopic methods (Tables 1 and 2). Use of the complexes $[W(\equiv CR)Cl(CO)_2L_2]$, as precursors for the synthesis of the salts (**1**), leads to significantly higher yields (*ca.* 70 compared with 20%) than if the compounds $[W(\equiv CR)Br(CO)_4]$ are used.

The i.r. spectra of the compounds (**1**) in the CO stretching region are very similar, consisting of two bands (Table 1). Both spectra also show a weak broad B–H stretch at *ca.* 2 524 cm^{-1}. It is interesting to compare the frequencies of the CO stretching bands in (**1**) at *ca.* 1 990 and 1 930 cm^{-1} with those in the spectra of the salts $[N(PPh_3)_2][W(\equiv CC_6H_4Me\text{-}4)(CO)_2(\eta^5\text{-}C_2B_9H_9Me_2)]$ (1 956 and 1 874 cm^{-1})[2a] and $[NEt_4][W(\equiv CC_6H_3Me_2\text{-}2,6)(CO)_2(\eta^5\text{-}C_2B_9H_9Me_2)]$ (1 958 and 1 877 cm^{-1}).[2h] The higher frequencies observed with the complexes (**1**) indicates that the $\eta^6\text{-}C_2B_{10}H_{10}Me_2$ group is more efficient than the $\eta^5\text{-}C_2B_9H_9Me_2$ moiety in delocalising the charge from the tungsten. This observation is consistent with electrochemical studies on homologous carbametallaboranes which indicate that the $\eta^5\text{-}C_2B_9H_{11}$ cage is a better donor than $\eta^6\text{-}C_2B_{10}H_{12}$. However, both cages can formally be regarded as four-electron donors to a metal centre.[2a,6a]

In the $^{13}C\text{-}\{^1H\}$ n.m.r. spectra of the salts (**1**) (Table 2), characteristic resonances for the ligated carbon atoms of the alkylidyne groups occur at δ 302.6 (**1a**) and 299.8 p.p.m. (**1b**). These shifts are very similar to those observed for the alkylidyne–carbon nuclei in the anions $[W(\equiv CR)(CO)_2(\eta^5\text{-}C_2B_9H_9Me_2)]^-$ [R = C_6H_4Me-4 (δ 298.3 p.p.m.) or $C_6H_3Me_2$-2,6 (δ 299.2 p.p.m.)].[2a,h] However, unlike the latter species, the compounds (**1**) undergo fluxional behaviour in solution, a property revealed by variable-temperature n.m.r. studies. However, discussion of this property is deferred until the results of an *X*-ray diffraction study on (**1b**) are presented.

The structure of the anion of (**1b**) is shown in Figure 1, and selected bond distances and angles are given in Table 3. It is readily apparent that the $C_2B_{10}H_{10}Me_2$ carbaborane cage is η^6-co-ordinated to the tungsten atom. A single boron atom [B(3)] separates the two carbon vertices in the face of the ligand as found in other metal complexes containing this group. Since the $C_2B_{10}W$ cage has 13 vertices there is a group of six atoms C(20)B(3)C(40)B(5)B(6)B(7) above the pentagonal B(8)—B(12)

Table 2. Hydrogen-1 and carbon-13 n.m.r. data[a] for the complexes

Compound	^1H[b,c] (δ)	^{13}C[d] (δ)
(**1a**)	1.21 [t, br, 12 H, NCH_2Me, *J*(HH) 7], 1.51 (s, 3 H, CMe), 2.28 (s, 3 H, Me-4), 2.84 (s, 3 H, CMe), 3.06 [q, 8 H, NCH_2Me, *J*(HH) 7], 7.12, 7.30[$(AB)_2$, 4 H, C_6H_4, *J*(AB) 8]	302.6 (C≡W), 213.9, 212.9 (CO), 148.1 [$C^1(C_6H_4)$], 139.1, 129.0, 128.3 (C_6H_4), 95.8, 63.9 (br, *C*Me), 52.0 (NCH_2Me), 37.9, 35.5 (C*Me*), 22.2 (Me-4), 7.7 (NCH_2Me)
(**1b**)	1.20 [t, 12 H, NCH_2Me, *J*(HH) 6], 1.53 (s, 3 H, CMe), 2.59 (s, 6 H, Me_2-2,6), 2.87 (s, 3 H, CMe), 3.02 [q, 8 H, NCH_2Me, *J*(HH) 7], 7.00, 7.18 [AB_2, 3 H, C_6H_3, *J*(AB) 8]	299.8 (C≡W), 215.1, 213.5 (CO), 146.9 [$C^1(C_6H_3)$], 140.8, 129.3, 127.4 (C_6H_3), 95.3, 63.6 (br, *C*Me), 52.0 (NCH_2Me), 37.5, 35.5 (C*Me*), 21.2 (Me_2-2,6), 7.7 (NCH_2Me)
(**2a**)	(i)[e,f] 2.02 (s, 3 H, CMe), 2.44 (s, 3 H, Me-4), 2.66 (s, 3 H, CMe), 7.24—7.70 (m, 19 H, C_6H_4, Ph)	(i) 280.5 [d, μ-C, *J*(PC) 27], 206.3, 204.3 (CO), 148.2 [$C^1(C_6H_4)$], 143.0, 134.7—127.2 (m, C_6H_4, Ph), 87.7, 76.6 (br, *C*Me), 37.9, 35.9 (C*Me*), 22.2 (Me-4)
	(ii)[f,g] 1.84 (s, 3 H, CMe), 2.44 (s, 3 H, Me-4), 2.51 (s, 3 H, CMe), 7.24—7.70 (m, 19 H, C_6H_4, Ph)	(ii) 296.8 [d, μ-C, *J*(PC) 34], 207.3, 206.0 (CO), 147.4 [$C^1(C_6H_4)$], 143.8, 134.7—127.2 (m, C_6H_4, Ph), 102.2, 76.1 (br, *C*Me), 40.5, 35.7 (C*Me*), 22.2 (Me-4)
(**2b**)	(i) 1.97, 2.23, 2.49, 2.71 (s × 4, 12 H, CMe, Me_2-2,6), 7.12—7.63 (m, 18 H, C_6H_3, Ph)	(i)[h,i] 276.8 [d, μ-C, *J*(PC) 29], 208.1, 203.5 [CO, *J*(WC) 159, 139, resp.], 149.8 [$C^1(C_6H_3)$], 139.9, 139.0 (C_6H_3), 134.8 [d, Ph, *J*(PC) 15], 132.9 (Ph), 130.1 [d, Ph, *J*(PC) 10], 129.2—128.1 (m, C_6H_3, Ph), 88.5 (*C*Me), 38.3, 35.8 (C*Me*), 22.6, 21.9 (Me_2-2,6)
	(ii) 1.78, 2.38, 2.46, 2.98 (s × 4, 12 H, CMe, Me_2-2,6), 7.12—7.63 (m, 18 H, C_6H_3, Ph)	(ii)[h,j] 282.9 [d, μ-C, *J*(PC) 26], 206.6 (CO), 149.6 [$C^1(C_6H_3)$], 138.9, 138.1 (C_6H_3), 38.7 (C*Me*), 22.4, 22.3 (Me_2-2,6)
(**3a**)	(i)[k] 1.65, 1.99, 2.42 (s × 3, 9 H, CMe, Me-4), 6.36—7.85 (m, 34 H, C_6H_4, Ph)	(i)[l] 211.1, 203.3 (CO), 158.2 [$C^1(C_6H_4)$], 138.6 (C_6H_4), 135.9—125.2 (m, C_6H_4, Ph), 86.6, 65.0 (br, *C*Me), 36.4, 34.5 (C*Me*), 21.9 (Me-4)
	(ii) 1.93, 2.46, 2.84 (s × 3, 9 H, CMe, Me-4), 6.36—7.85 (m, 34 H, C_6H_4, Ph)	(ii)[j,l] 208.9 (CO), 151.7 [$C^1(C_6H_4)$], 141.7 (C_6H_4), 37.0, 35.9 (C*Me*)
(**3b**)	[m] 1.45, 1.66, 2.11, 2.57 (s × 4, 12 H, CMe, Me_2-2.6), 7.06—7.52 (m, 33 H, C_6H_3, Ph)	[m,n] 357.5 (m, μ-C), 257.1 [d, μ-CO, *J*(RhC) 26], 202.4 [d, CO, *J* 6], 152.4 [$C^1(C_6H_3)$], 139.4, 136.7 (C_6H_3), 134.1, 133.6 [d × 2, Ph, *J*(PC) 11], 131.1, 130.8 (Ph), 129.2, 129.0 (C_6H_3), 128.7, 128.6, 128.5 (Ph), 94.8, 70.3 (br, *C*Me), 36.6, 35.1 (C*Me*), 23.7, 22.2 (Me_2-2,6)
(**4**)	[o] 1.34 [t, br, 12 H, NCH_2Me, *J*(HH) 6], 1.94, 2.40, 2.65 (s × 3, 9 H, CMe, Me-4), 3.19 [q, 8 H, NCH_2Me, *J*(HH) 7], 7.13, 7.26 [$(AB)_2$, 4 H, C_6H_4, *J*(AB) 7]	[o] 300.5 (μ-C), 216.6 (WCO), 214.5, 214.2 (FeCO), 212.4 (WCO), 159.7 [$C^1(C_6H_4)$], 135.9, 128.0, 127.7 (C_6H_4), 69.8, 59.2 (br, *C*Me), 53.2 (NCH_2Me), 36.4, 35.6 (C*Me*), 21.2 (Me-4), 7.8 (NCH_2Me)
(**5**)	[m,p] −0.4 [q, br, 1 H, B(μ-H)Fe, *J*(BH) 84], 1.39 [t of t, 12 H, NCH_2Me, *J*(NH) 2, *J*(HH) 7], 1.62, 1.71, 1.87, 2.17 (s × 4, 12 H, CMe, Me_2-2,6), 3.52 [q, 8 H, NCH_2Me, *J*(HH) 7], 7.05—7.25 (m, 3 H, C_6H_3)	[m] 369.2 [μ-C, *J*(WC) 113], 219.6, 216.8 (FeCO), 213.3, 202.5 [WCO, *J*(WC) 130, 153, resp.], 164.8 [$C^1(C_6H_3)$], 128.1, 127.8, 127.2, 126.7, 125.2 (C_6H_3), 76.9, 63.4 (br, *C*Me), 52.6 (NCH_2Me), 36.5, 34.5 (C*Me*), 21.1, 21.0 (Me_2-2,6), 7.8 (NCH_2Me)

[a] Chemical shifts (δ) in p.p.m., coupling constants in Hz; all measurements at −80 °C unless otherwise stated. [b] Measured in CD_2Cl_2 unless otherwise stated. [c] Proton resonances for BH groups occur as broad unresolved signals in the range δ 0—3 p.p.m. [d] Hydrogen-1 decoupled, chemical shifts are positive to high frequency of $SiMe_4$, with measurements in CD_2Cl_2–CH_2Cl_2 unless otherwise stated. [e] Peaks for major isomer. [f] Measured at −86 °C. [g] Peaks for minor isomer. [h] In CD_2Cl_2–thf (1:2). [i] Second *C*Me resonance for major isomer lies under thf peak. [j] Some resonances for the minor isomer occur under the signals for the major isomer. [k] B(μ-H)Rh signal not observed due to coupling with ^{11}B, ^{103}Rh, and ^{31}P nuclei. [l] μ-*C*C_6H_4Me-4 resonance not observed due to low solubility, and coupling with ^{103}Rh and ^{31}P nuclei. [m] Measured at −40 °C. [n] The remaining C_6H_3 ring carbon signal occurs under resonances for PPh_3. [o] Measured at room temperature. [p] In $(CD_3)_2CO$.

Table 3. Selected internuclear distances (Å) and angles (°) for the complex $[NEt_4][W(\equiv CC_6H_3Me_2\text{-}2,6)(CO)_2(\eta^6\text{-}C_2B_{10}H_{10}Me_2)]$ (**1b**)

W–C(1)	1.84(1)	W–C(01)	2.00(1)	W–C(02)	2.01(1)	W–C(20)	2.26(1)
W–C(40)	2.56(1)	W–B(7)	2.44(1)	W–B(3)	2.50(1)	W–B(5)	2.39(1)
W–B(6)	2.46(1)	C(20)–B(7)	1.54(2)	C(20)–B(3)	1.54(2)	C(20)–B(8)	1.81(2)
C(40)–B(3)	1.69(2)	C(40)–B(5)	1.75(2)	C(40)–B(10)	1.69(2)	C(40)–B(9)	1.68(2)
B(6)–B(7)	1.79(2)	B(7)–B(12)	1.77(2)	B(3)–B(9)	1.81(2)	B(5)–B(6)	1.79(2)
B(5)–B(11)	1.76(2)	B(5)–B(10)	1.80(2)	B(6)–B(12)	1.78(2)	B(6)–B(11)	1.78(2)
B(8)–B(12)	1.89(2)	B(11)–B(12)	1.79(2)	B(12)–B(13)	1.73(2)	B(8)–B(9)	1.87(3)
B(8)–B(13)	1.80(2)	B(10)–B(11)	1.73(2)	B(11)–B(13)	1.81(2)	B(9)–B(10)	1.70(2)
B(10)–B(13)	1.76(3)	B(9)–B(13)	1.72(3)	B(7)···B(8)	1.98(2)	B(3)···B(8)	1.99(2)
C(20)–C(21)	1.53(2)	C(40)–C(41)	1.52(2)	C(1)–C(2)	1.42(1)	C(01)–O(01)	1.14(2)
C(02)–O(02)	1.14(2)						
W–C(01)–O(01)	178(1)	W–C(02)–O(02)	178(1)	W–C(1)–C(2)	175.6(9)	C(01)–W–C(1)	83.0(5)
C(02)–W–C(1)	87.7(5)	C(1)–W–C(40)	164.7(4)	C(1)–W–B(3)	154.5(5)	C(1)–W–C(20)	118.5(4)
C(01)–W–C(20)	156.9(5)	C(01)–W–B(7)	153.9(6)	C(02)–W–B(6)	159.6(6)	C(02)–W–B(5)	144.8(5)
C(01)–W–C(02)	89.2(6)						

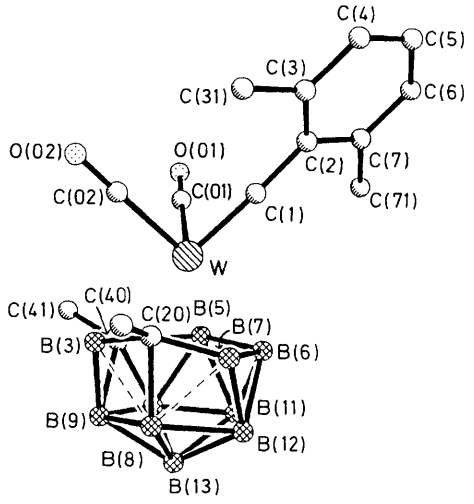

Figure 1. The structure of the anion of $[NEt_4][W(\equiv CC_6H_3Me_2\text{-}2,6)(CO)_2(\eta^6\text{-}C_2B_{10}H_{10}Me_2)]$ (**1b**), showing the crystallographic numbering

ring. This leads to distortions within the framework of the cage, which are not observed in 12-vertex carbametallaboranes. These distortions take two forms: there is a distinctly non-planar ring of boron and carbon atoms in the face of the cage attached to the metal, and also deviations occur from the symmetrical triangulated faces found in icosahedral structures. Similar distortions have been observed in the structures of $[NMe_4]_2[Ti(\eta^6\text{-}C_2B_{10}H_{10}Me_2)_2]$,[6b] $[Co(\eta\text{-}C_5H_5)(\eta^6\text{-}C_2B_{10}H_{12})]$,[6c] $[RhH(PPh_3)_2(\eta^6\text{-}C_2B_{10}H_{12})]$,[6d] $[Pd(Ph_2PCH_2CH_2PPh_2)(\eta^6\text{-}C_2B_{10}H_{12})]$,[7] and $[IrH(PPh_3)_2\{\eta^6\text{-}C_2B_{10}H_{11}(OMe)\}]$.[7]

The non-planar co-ordination face of the carbaborane ligand in (**1b**) is associated with a 0.30 Å difference in the connectivities involving the two carbon atoms and the tungsten atom [W–C(20) 2.26(1), W–C(40) 2.56(1) Å]. The W–B connectivities lie between these two extremes: W–B(3) 2.50(1), W–B(5) 2.39(1), W–B(6) 2.46(1), and W–B(7) 2.44(1) Å. Interestingly, in (**1b**) it is C(40), transoid to the alkylidyne group [C(1)–W–C(40) 164.7(4)°], which is furthest from the tungsten. It is likely, therefore, that the *trans* influence of the alkylidyne ligand will have reinforced the non-planarity of the C(20)B(3)C(40)B(5)B(6)B(7) ring.

The carbaborane cage co-ordination may be compared with those observed in the aforementioned complexes of Ti, Co, Pd, and Ir. In all the structures, including (**1b**), the shortest connectivity between the metal and the ring involves a carbon atom. Distortions in the triangulated faces associated with this carbon atom, discussed below for (**1b**), lead to it being in a low-connectivity site. This is consistent with structural studies on a variety of polyhedral carbametallaboranes which reveal a distinct preference for cage carbon atoms to occupy low connectivity sites.[8]

Although in docosahedral structures a carbon vertex is involved in the shortest connectivity to the metal, the longest connectivity can be between the metal and either a carbon or a boron atom. As mentioned above, for (**1b**) it is the carbon atom C(40) in the face of the ligand which is furthest from the tungsten whereas in $[IrH(PPh_3)_2\{\eta^6\text{-}C_2B_{10}H_{11}(OMe)\}]$ it is a boron atom in the η^6-ligating ring which is furthest [2.520(15) Å] from the iridium.[7] This boron atom, however, is transoid to a hydrido group, and it is probably the *trans* influence of the ligand which is responsible for the effect.

In (**1b**), the B(3)···B(8) [1.99(2) Å] and B(7)···B(8) [1.98(2) Å] separations are distinctly longer than the other B–B distances in the cage, and these connectivities have therefore been represented by dashed lines. The relatively long B(3)···B(8) and B(7)···B(8) separations result in two essentially square faces centred around C(20), *viz.* C(20)B(3)B(9)B(8) and C(20)B(7)B(12)B(8). Moreover, C(20) has a connectivity of four, excluding its exopolyhedral methyl group, and B(8) a connectivity of six excluding its exopolyhedral hydrogen atom. These connectivities are one less and one more, respectively, than those encountered in the triangulated carbametallaboranes.[8] The difference in connectivities at the C(20) and B(8) vertices in (**1b**) is due to the presence of a sixth atom in the face of the cage, a situation which does not occur in complexes of the $\eta^5\text{-}C_2B_9H_9Me_2$ group. As the connectivities around a particular atom increase the average separations with its neighbours lengthen.[6c] This is manifested in the connectivities involving B(8). In addition to the longer distances to B(3) and B(7), the connectivities B(8)–B(9) [1.87(3)] and B(8)–B(12) [1.89(2) Å] are also appreciably greater than normal (*ca.* 1.78 Å). The opposite situation occurs at the C(20) vertex, the C(20)–B(3) and C(20)–B(7) distances being relatively short [1.54(2) Å]. The C(20)–W bond [2.26(1) Å] is also short. The latter separation may be compared with the appreciably longer carbon–tungsten distances [2.385(6) and 2.474(7) Å] in the anion $[W(\equiv CC_6H_4Me\text{-}4)(CO)_2(\eta^5\text{-}C_2B_9H_9Me_2)]^-$, which contains the icosahedral C_2B_9W group with a planar pentagonal face.[9]

Among the various docosahedral carbametallaborane structures established by *X*-ray crystallography there are distinct differences in the dimensions of the 'non-triangulated' faces. Thus in (**1b**), and $[Ti(\eta^6\text{-}C_2B_{10}H_{10}Me_2)_2]^{2-}$,[6b] the diagonals across these faces (*ca.* 1.99 Å) are essentially the same. However, in $[Pd(Ph_2PCH_2CH_2PPh_2)(\eta^6\text{-}C_2B_{10}H_{12})]$ and $[IrH(PPh_3)_2\{\eta^6\text{-}C_2B_{10}H_{11}(OMe)\}]$ the B···B diagonal distances are distinctly asymmetric, being, respectively, 1.911(7) and 2.173(7) Å for the palladium compound, and 1.90(3) and 2.33(3) Å for the iridium complex.[7] It is interesting to note that in $[RhH(PPh_3)_2(\eta^6\text{-}C_2B_{10}H_{12})]$ the distortion in the docosahedron is confined to one face, the B···B diagonal being 2.166 Å.[6d]

In (**1b**) the remaining co-ordination sites on tungsten are occupied by two terminal CO groups and the xylylmethylidyne ligand [W–C(1) 1.84(1) Å]. The W–C(1)–C(2) group [175.6(9)°] deviates only slightly from linearity. Indeed the bonding of the alkylidyne fragment to the metal in (**1b**) is very similar to that in $[W(\equiv CC_6H_4Me\text{-}4)(CO)_2(\eta^5\text{-}C_2B_9H_9Me_2)]^-$ [C≡W 1.826(7) Å, W≡C–C 178.4(4)°].[9]

As mentioned earlier, the complexes (**1**) undergo dynamic behaviour in solution. The ^1H n.m.r. spectra of (**1a**) and (**1b**), measured at room temperature, each show two Me group signals (aryl-methyl and CMe) even though the *X*-ray diffraction study on (**1b**) revealed that in the solid state the two methyl substituents on the cage are in different environments. In the spectra measured at ambient temperatures the resonances [δ 2.17 (**1a**) and 2.20 (**1b**)] for the CMe groups are broad, and at −30 °C these peaks collapse into the baseline. On further cooling to −80 °C, two new singlet signals [δ 1.51 and 2.84 (**1a**), 1.53 and 2.87 (**1b**)] appear, each corresponding to three protons. The $^{13}C\text{-}\{^1H\}$ n.m.r. spectra also vary with temperature. At room temperature, both complexes show a single CO resonance [δ 214.3 (**1a**) and 215.2 p.p.m. (**1b**)]. However, the spectra measured at −80 °C show two CO peaks [δ 212.9 and 213.9 (**1a**), and 213.5 and 215.1 p.p.m. (**1b**)]. Thus the pattern observed in the spectra measured at low temperatures is in agreement with the asymmetry revealed by the *X*-ray diffraction study of (**1b**).

The dynamic behaviour occurring in the salts (**1**) in solution is readily interpreted by the process shown in the Scheme. The CMe fragments change their relationship with the tungsten atom *via* a diamond–square–diamond polytopal rearrangement

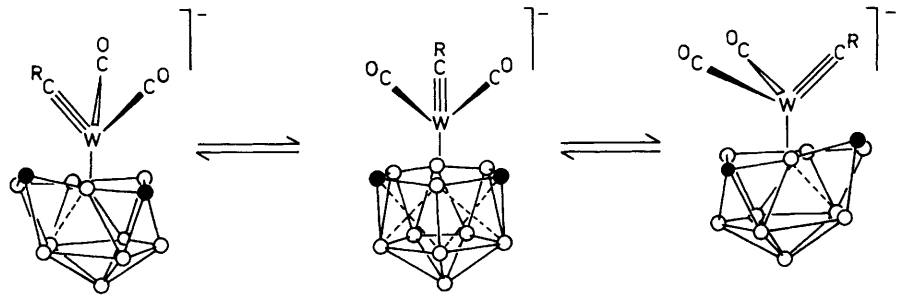

Scheme.

of the cage.[4] This is accompanied by a concomitant rotation of the W(≡CR)$(CO)_2$ (R = C_6H_4Me-4 or $C_6H_3Me_2$-2,6) moiety. The latter process enables the two CMe units to alternate between transoid and non-transoid sites with respect to the alkylidyne group.

Several reactions of the salts (**1**) have been investigated. Treatment of thf solutions with [AuCl(PPh_3)], in the presence of KPF_6, affords the dimetal compounds [WAu(μ-CR)$(CO)_2$(PPh_3)(η⁶-$C_2B_{10}H_{10}Me_2$)] [R = C_6H_4Me-4 (**2a**) or $C_6H_3Me_2$-2,6 (**2b**)]. These complexes, characterised by the data given in Tables 1 and 2, are analogues of the previously reported compounds [WAu(μ-CR)$(CO)_2$(PPh_3)(η⁵-$C_2B_9H_9Me_2$)] (R = Me, C_6H_4Me-2, C_6H_4Me-4, or $C_6H_3Me_2$-2,6).[2a,h] An *X*-ray diffraction study[2a] on [WAu(μ-CC_6H_4Me-4)$(CO)_2$(PPh_3)(η⁵-$C_2B_9H_9Me_2$)] revealed that the *p*-tolylmethylidyne group semi-bridges the metal–metal bond, being much more closely bound to the tungsten. It is likely that the alkylidyne groups also asymmetrically bridge the W–Au bonds in (**2**).

The compounds (**2**) are formed as mixtures of two isomers, with each isomer undergoing fluxional behaviour of the kind discussed above for the anions of (**1**). The ^1H n.m.r. spectra of (**2a**) and (**2b**), when measured at room temperature, show only one broad resonance for the cage CMe groups [δ 2.28 (**2a**) and 2.33 (**2b**)]. At −80 °C the spectrum of (**2a**) displays two sets of CMe signals. These are at δ 2.02 and 2.66 for the major isomer, and at δ 1.84 and 2.51 for the minor isomer. Relative peak intensities indicated that the two isomers are formed in a ratio of *ca.* 3:2. Not surprisingly the Me-4 resonances for both isomers were the same (δ 2.44). Interestingly, the ^1H n.m.r. spectrum of (**2b**) at −80 °C showed two sets of four resonances (Table 2) since for each isomer (ratio 4:1) not only are the cage CMe groups non-equivalent, but the xylyl Me_2-2,6 groups are also. Evidently the asymmetry inherent in the docosahedral $C_2B_{10}W$ framework is responsible for this effect.

The ^{13}C-{^1H} n.m.r. spectra measured at −80 °C also confirm the presence of two isomers for each complex. In the spectrum of (**2a**) two alkylidyne-carbon resonances occur at δ 280.5 and 296.8 p.p.m., and these signals can be assigned to the major and minor isomers, respectively, on the basis of peak intensities. In the spectrum of (**2b**) the corresponding resonances for the two isomers occur at δ 276.8 and 282.9 p.p.m. Moreover, in accord with the existence of two isomers, four CO peaks appear in the spectrum of (**2a**) [δ 206.3 and 204.3 (major isomer), δ 207.3 and 206.0 p.p.m. (minor isomer)], and three in the spectrum of (**2b**) [δ 208.1 and 203.5 (major isomer), δ 206.6 p.p.m. (minor isomer; second signal obscured by that for the major isomer)].

The data can be interpreted in terms of each isomer undergoing fluxional behaviour of the carbaborane cage similar to that occurring in the anions of (**1**), accompanied by a rotation of the WAu(μ-CR)$(CO)_2$(PPh_3) groups. The fact that the i.r. spectra of the complexes (**2**) display only two CO stretches (Table 1) indicates that the isomers of each species have similar CO ligand environments. Hence isomerism based on transoid and cisoid arrangements of the η⁶-$C_2B_{10}H_{10}Me_2$ and CR groups with respect to the W–Au bond can be ruled out. It is proposed, therefore, that the isomerism relates to two different orientations of the carbaborane cage, so that in one isomer a cage-carbon atom is transoid to the μ-CR group and in the other a cage-boron atom is transoid to this group. In the latter isomer, the boron atom would be involved in the long cage–metal connectivity, due to the *trans* influence of the alkylidyne ligand. This situation occurs in [Co(η-C_5H_5)(η⁶-$C_2B_{10}H_{12}$)][6c] and [IrH(PPh_3)$_2${η⁶-$C_2B_{10}H_{11}$(OMe)}].[7] These complexes have boron–metal connectivities [2.203(4) (Co), 2.520(15) Å (Ir)] which are the longest of the various cage-to-metal linkages. It is uncertain which of the possible four boron atoms in (**2**) would occupy the long connectivity site, transoid to the μ-CR group. However, it is unlikely to be the unique boron atom [B(6) in Figure 1] which is only attached in the cage to other boron atoms, since this would direct the CMe groups towards the bulky Au(PPh_3) fragment.

It is interesting to note that the previously reported compounds [WAu(μ-CR)$(CO)_2$(PPh_3)(η⁵-$C_2B_9H_9Me_2$)] do not exist as isomeric mixtures, nor do they undergo fluxional behaviour in solution. In their ^{13}C-{^1H} n.m.r. spectra, the μ-C resonances occur at δ 292.9 (μ-CC_6H_4Me-4)[2a] and 284.5 p.p.m. (μ-$CC_6H_3Me_2$-2,6).[2h] The corresponding signals (δ 276.8—296.8 p.p.m.) for the isomers of (**2a**) and (**2b**) are also relatively shielded for metal compounds with bridging alkylidyne groups,[10,11] and these shifts are diagnostic for complexes in which the μ-CR ligands asymmetrically bridge a metal–metal bond.[2i]

Earlier studies[2a] showed that the reaction between [Rh(cod)(PPh_3)$_2$][PF_6] (cod = cyclo-octa-1,5-diene) and [N(PPh_3)$_2$][W(≡CC_6H_4Me-4)$(CO)_2$(η⁵-$C_2B_9H_9Me_2$)] gives the tungsten–rhodium complex [WRh(μ-CC_6H_4Me-4)$(CO)_2$(PPh_3)$_2$(η⁵-$C_2B_9H_9Me_2$)]. It was of interest, therefore, to investigate reactions between the salts (**1**) and [Rh(cod)(PPh_3)$_2$][PF_6]. In this manner the complexes [WRh(μ-CR)$(CO)_2$(PPh_3)$_2$(η⁶-$C_2B_{10}H_{10}Me_2$)] [R = C_6H_4Me-4 (**3a**) and $C_6H_3Me_2$-2,6 (**3b**)] were isolated in high yield, and characterised by the data given in Tables 1 and 2.

The i.r. spectra of (**3a**) and (**3b**) in the CO stretching region are distinctly different. That of (**3b**) consists of two bands at 2 010 and 1 787 cm^{-1}. These absorptions are very similar to those observed[2a] in the spectrum of [WRh(μ-CC_6H_4Me-4)$(CO)_2$(PPh_3)$_2$(η⁵-$C_2B_9H_9Me_2$)] at 1 961 and 1 767 cm^{-1}. The two complexes are therefore presumed to have similar structures, which in the case of the species containing the ligand

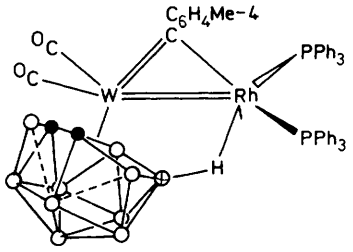

(i)

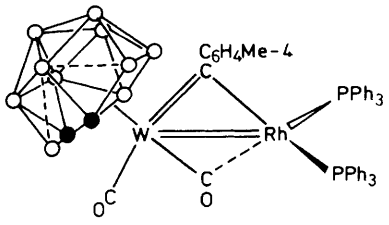

(ii)

(3a)

○ BH ⊕ B ● CMe

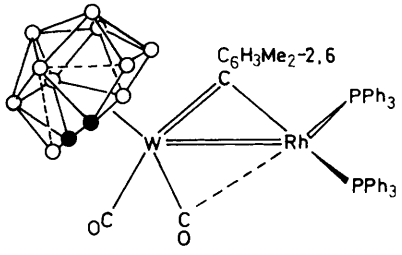

(3b)

η^5-$C_2B_9H_9Me_2$ has been confirmed by *X*-ray diffraction. The latter study [2a] revealed that one of the CO groups semi-bridged the W–Rh bond. However, as discussed earlier, the i.r. band at 1 767 cm^{-1} is at such a low frequency as to suggest that in solution the CO ligand is fully bridging, and this may be the situation for (**3b**) also. In contrast with (**3b**), the i.r. spectrum of compound (**3a**) shows four CO absorptions at 2 001, 1 987, 1 962, and 1 808 cm^{-1}, and this observation provided the first evidence that the latter was formed as a mixture of two isomers.

Variable-temperature ^1H and ^{13}C-{^1H} n.m.r. studies showed that both complexes (**3**) underwent fluxional behaviour involving the η^6-$C_2B_{10}H_{10}Me_2$ cage framework of the type discussed previously. Moreover, the data for (**3a**) (Table 2) confirmed the existence in solution of an equilibrium between two isomers (ratio *ca.* 3:1), first indicated by the i.r. measurements. The ^1H n.m.r. spectrum of (**3a**) at room temperature consisted, apart from aromatic proton signals, of a singlet peak at δ 2.40 assigned to the tolylmethylidyne Me-4 group. Resonances due to the cage CMe groups were not observed. In the spectrum measured at −30 °C two Me-4 signals were found at δ 2.40 and 2.43. Moreover, peaks appeared (δ 1.66 and 1.99) which could be assigned to the carbaborane CMe fragments of the major isomer. Further cooling to −60 °C results in the appearance of two additional singlets (δ 1.94 and 2.82). Finally, at −80 °C, the spectrum in the methyl group region consists of two distinct sets of three singlet signals due to the Me-4 and CMe groups of each isomer. Interestingly, the measurements show that the fluxional behaviour of the major isomer ceases at *ca.* −30 °C, whereas the limiting spectrum of the minor isomer was not attained much above −80 °C.

The ^{13}C-{^1H} n.m.r. spectrum of (**3a**) (Table 2) at −80 °C was less informative, due to low solubility and coupling of ^{13}C signals with ^{31}P and ^{103}Rh nuclei. Thus the μ-C resonances were not observed. However, CO peaks for the major isomer were seen at δ 211.1 and 203.3 p.p.m., and a resonance for the terminal carbonyl ligand in the minor isomer occurred at δ 208.9 p.p.m. The structure of the major isomer of (**3a**) was revealed by inspection of the ^{11}B-{^1H} and ^{11}B spectra. The ^{11}B-{^1H} spectrum of the isomeric mixture revealed a well resolved resonance at δ 21.8 p.p.m., all other boron nuclei giving rise to a broad band at *ca.* δ −7.1 p.p.m. In a ^{11}B spectrum the signal at δ 21.8 p.p.m. became a doublet [*J*(BH) 73 Hz]. These data establish the presence of a B–H→Rh three-centre two-electron bond involving a BH vertex in the tungsten-ligating face of the η^6-$C_2B_{10}H_{10}Me_2$ group. In studies involving the ligand η^5-$C_2B_9H_9Me_2$ we have identified several examples of e-exopolyhedral bonding of this type.[2b–e,i] In the complex [WRu(μ-CC_6H_4Me-4)$(CO)_3(\eta$-$C_5H_5)(\eta^5$-$C_2B_9H_9Me_2)$], which has a B–H→Ru linkage, the ^{11}B-{^1H} n.m.r. resonance for the unique boron nucleus is at δ 19.5 p.p.m., very similar in chemical shift to that assigned to the boron atom of the B–H→Rh group in (**3a**) [isomer (i)]. In the ^1H n.m.r. spectrum the signal for the μ-H proton was not observed, but this is not surprising since the signal would be broadened by the ^{11}B nucleus and split by ^{103}Rh and ^{31}P coupling. It is uncertain which BH vertex partakes in B–H→Rh bonding. However, based on earlier work [2b–e,i] which showed a preference with the η^5-$C_2B_9H_9Me_2$ ligand for involvement of the central boron $\overline{CCB\mathit{B}B}$ in the face of the cage, it seems likely that it is the 'central' boron $\overline{CBCB\mathit{B}B}$ also in the docosahedral cage which engages in this mode of exopolyhedral bonding to the adjacent metal atom. To the best of our knowledge the major isomer (i) of (**3a**) is the first example of a 13-vertex polyhedral species having a B–H→metal bond.

The minor isomer (ii) of (**3a**) almost certainly has a structure similar to those of (**3b**) and [WRh(μ-CC_6H_4Me-4)$(CO)_2$-$(PPh_3)_2(\eta^5$-$C_2B_9H_9Me_2)$].[2a] The interconversion of the two isomers of (**3a**) would thus involve dissociation of the B–H→Rh interaction in the major isomer in a reversible manner. In the minor isomer the η^6-$C_2B_{10}H_{10}Me_2$ ligand would adopt a spectator role. Similar behaviour occurs with the complex [WIr(μ-CC_6H_4Me-4)$(CO)_2(PEt_3)_2(\eta^5$-$C_2B_9H_9Me_2)$], which when dissolved in polar solvents exists as a mixture of isomers

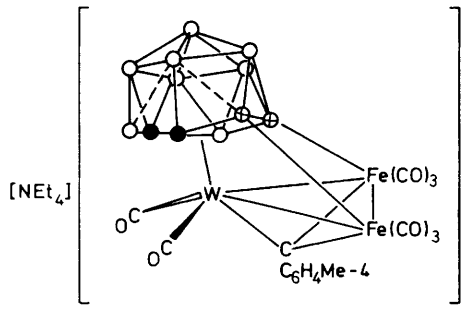

(4)

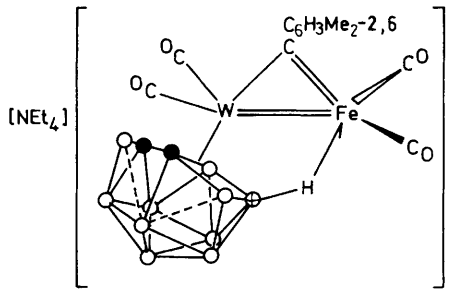

(5)

○ BH ⊕ B ● CMe

having structures both with and without a B–H→Ir bond.[12] The major isomer of (**3a**) may be favoured because with this structure both metal centres acquire filled 18-electron shells, whereas in the minor isomer the rhodium atom has a 16-electron shell.

As mentioned above, complex (**3b**) undergoes rapid exchange in solution between two equivalent structures. This fluxionality, shown by the majority of the other complexes reported herein, is associated with diamond–square–diamond transformations within the docosahedral framework. The ^{1}H n.m.r. spectrum of (**3b**) measured at −40 °C shows four methyl-group resonances. Therefore, as in compound (**2b**), the asymmetry inherent in the C_2B_{10} cage renders the xylyl methyl substituents inequivalent. This is supported by the ^{13}C-{^{1}H} n.m.r. spectrum (Table 2) which shows not only two resonances for the Me_2-2,6 groups but also five peaks for the carbon nuclei of the aromatic ring, the sixth signal being masked by other resonances. As noted previously the minor isomer of (**3a**), structurally akin to (**3b**), is fluxional at lower temperatures than the major isomer. This is consistent with the presence of the B–H→Rh bond in the major isomer making the framework more rigid.

The alkylidyne-carbon resonance of (**3b**) (357.5 p.p.m.) is barely observable as a multiplet, due to unresolved coupling with ^{103}Rh and ^{31}P nuclei. The resonance at δ 257.1 p.p.m. [*J*(RhC) 26 Hz] may be assigned to the semi-bridging CO group. The signal for the terminal CO group (202.4 p.p.m.) is also a doublet (*J* 6 Hz), but it is uncertain whether this coupling is due to ^{31}P or ^{103}Rh, although the latter seems more likely.

It is interesting that no second isomer of (**3b**) exists which is structurally similar to the major isomer of (**3a**). Subtle electronic differences between the μ-CC_6H_4Me-4 and μ-$CC_6H_3Me_2$-2,6 groups must be responsible. Steric differences seem unlikely to be the cause of this difference since the presence of the xylyl group in (**3b**) might well favour a structure where the carbaborane cage is more transoid to the alkylidyne group, as in the major isomer of (**3a**).

The ^{31}P-{^{1}H} n.m.r. spectra of the compounds (**3**) were measured at −80 °C. That of (**3a**) showed two signals for each isomer, each a doublet of doublets: major isomer, δ 52.2 [*J*(PP) 29, *J*(RhP) 162] and 38.5 p.p.m. [*J*(PP) 28, *J*(RhP) 148 Hz]; minor isomer, δ 41.3 [*J*(PP) 26, *J*(RhP) 172 Hz], and 27.8 p.p.m. [*J*(PP) 25, *J*(RhP) 146 Hz]. The spectrum of (**3b**), as expected for the non-equivalent PPh_3 groups, also shows two doublet of doublets: δ 33.2 [*J*(PP) 32, *J*(RhP) 169] and 26.5 p.p.m. [*J*(PP) 32, *J*(RhP) 146 Hz].

In view of the variety of products obtained on treatment of the salts $[NEt_4][W(\equiv CR)(CO)_2(\eta^5\text{-}C_2B_9H_9Me_2)]$ (R = C_6H_4-Me-4 or $C_6H_3Me_2$-2,6) with iron carbonyls,[2g,h] reactions between the salts (**1**) and $[Fe_2(CO)_9]$ were investigated. Treatment of (**1a**) with $[Fe_2(CO)_9]$ affords the trimetal complex $[NEt_4][WFe_2(\mu_3\text{-}CC_6H_4Me\text{-}4)(\mu\text{-}\sigma\text{:}\sigma'\text{:}\eta^6\text{-}C_2B_{10}H_8Me_2)(CO)_8]$ (**4**), characterised by the data given in Tables 1 and 2. Compound (**4**) is closely related to the complex $[NEt_4][WFe_2(\mu_3\text{-}CC_6H_4Me\text{-}4)(\mu\text{-}\sigma\text{:}\sigma'\text{:}\eta^5\text{-}C_2B_9H_7Me_2)(CO)_8]$, a product of the reaction of $[NEt_4][W(\equiv CC_6H_4Me\text{-}4)(CO)_2(\eta^5\text{-}C_2B_9H_9Me_2)]$ with $[Fe_2(CO)_9]$. Interestingly, this reaction also affords a dimetal compound $[NEt_4][WFe\{\mu\text{-}CH(C_6H_4Me\text{-}4)\}(\mu\text{-}\sigma\text{:}\eta^5\text{-}C_2B_9H_8Me_2)(\mu\text{-}CO)(CO)_5]$. A similar species, with a bridging alkylidene group, was not formed in the reaction of (**1a**) with $[Fe_2(CO)_9]$.

Compound (**4**) does not undergo fluxional behaviour at ambient temperatures of the type discussed earlier since in the ^{1}H n.m.r. spectrum peaks for the two non-equivalent cage CMe groups are observed. In the ^{13}C-{^{1}H} n.m.r. spectrum these groups show resonances at δ 69.8 and 59.2 (*C*Me), and 36.4 and 35.6 p.p.m. (C*Me*), as expected for the asymmetric structure shown. The ^{13}C-{^{1}H} n.m.r. spectrum also showed four CO resonances. Those at δ 216.6 and 212.4 p.p.m., each correspond to one CO ligand and are assigned to the $W(CO)_2$ group. The peaks at δ 214.5 and 214.2 p.p.m. each correspond in intensity to *ca.* three CO groups, and are assigned to the two $Fe(CO)_3$ moieties. These groups are evidently undergoing rotation on the n.m.r. time-scale, leading to carbonyl site exchange. A similar resonance pattern is displayed by the CO groups in $[NEt_4][MoFe_2(\mu_3\text{-}CC_6H_4Me\text{-}4)(\mu\text{-}\sigma\text{:}\sigma'\text{:}\eta^5\text{-}C_2B_9H_7Me_2)(CO)_8]$.[1]

In the ^{13}C-{^{1}H} n.m.r. spectrum of (**4**) the signal for the μ-C nucleus occurs at δ 300.5 p.p.m. Surprisingly, this chemical shift is significantly more deshielded than the corresponding peak (δ 273.0 p.p.m.) in the spectrum of $[NEt_4][WFe_2(\mu_3\text{-}CPh)(\mu\text{-}\sigma\text{:}\sigma'\text{:}\eta^5\text{-}C_2B_9H_7Me_2)(CO)_8]$.[2g] An *X*-ray diffraction study established the structure of the latter complex, and this revealed that the CPh ligand symmetrically caps the metal triangle. The observed difference in the n.m.r. chemical shifts for the μ_3-C nuclei between the above two WFe_2 species may be due to the CC_6H_4Me-4 ligand in (**4**) asymmetrically bridging the metal triangle.[13] Alternatively, the difference in the chemical shifts may arise through different electronic properties of the C_2B_9 and C_2B_{10} carbaborane frameworks. An *X*-ray diffraction study[14] was carried out on (**4**) in an attempt to resolve this matter. Unfortunately, poor crystal quality prevented a precise determination of the structural parameters but the overall geometry of the anion was established showing that the C_2B_{10} cage had slipped over the face of the WFe_2 core on the opposite side to the *p*-tolylmethylidyne group.

The ^{11}B-{^{1}H} n.m.r. spectrum of complex (**4**) confirmed the presence of the two B–Fe σ bonds with diagnostic resonances at δ 47.3 and 58.8 p.p.m. These signals remained as singlets in a ^{1}H-coupled spectrum, confirming the absence of a proton

Table 4. Selected internuclear distances (Å) and angles (°) for the complex $[NEt_4][WFe(\mu\text{-}CC_6H_3Me_2\text{-}2,6)(CO)_4(\eta^6\text{-}C_2B_{10}H_{10}Me_2)]$ (**5**)

W–Fe	2.512(2)	W–C(1)	2.02(1)	Fe–C(1)	1.82(1)	W–C(01)	2.00(1)
W–C(02)	1.98(2)	Fe–C(03)	1.73(2)	Fe–C(04)	1.74(1)	W–C(20)	2.19(1)
W–B(3)	2.46(2)	W–C(40)	2.51(1)	W–B(5)	2.35(1)	W–B(6)	2.33(1)
W–B(7)	2.44(1)	Fe–B(6)	2.20(1)	Fe–Hb(6)	1.7(1)	B(6)–Hb(6)	1.3(1)
C(20)–B(3)	1.58(2)	B(3)–C(40)	1.71(2)	C(40)–B(5)	1.73(2)	B(5)–B(6)	1.75(2)
B(6)–B(7)	1.83(2)	B(7)–C(20)	1.56(2)	C(20)–B(8)	1.76(2)	B(7) · · · B(8)	1.97(2)
B(3) · · · B(8)	2.00(2)	B(3)–B(9)	1.82(2)	C(40)–B(9)	1.71(2)	C(40)–B(10)	1.69(2)
B(5)–B(10)	1.81(2)	B(5)–B(11)	1.81(2)	B(6)–B(11)	1.74(2)	B(6)–B(12)	1.72(2)
B(7)–B(12)	1.77(2)	B(8)–B(9)	1.87(3)	B(9)–B(10)	1.71(2)	B(10)–B(11)	1.79(2)
B(11)–B(12)	1.71(2)	B(8)–B(12)	1.89(3)	B(8)–B(13)	1.84(3)	B(9)–B(13)	1.76(3)
B(10)–B(13)	1.77(2)	B(11)–B(13)	1.79(2)	B(12)–B(13)	1.76(3)	C(1)–C(2)	1.46(2)
W–C(1)–Fe	81.4(4)	W–Fe–C(1)	52.8(3)	Fe–W–C(1)	45.8(3)	W–C(1)–C(2)	147.8(8)
Fe–C(1)–C(2)	130.9(8)	C(01)–W–C(02)	82.2(6)	Fe–W–C(01)	109.8(4)	Fe–W–C(02)	121.7(5)
W–Fe–C(03)	133.7(4)	W–Fe–C(04)	131.0(5)	C(1)–W–C(01)	89.4(4)	C(1)–W–C(02)	79.0(6)
C(1)–Fe–C(03)	100.4(6)	C(1)–Fe–C(04)	106.4(6)	C(1)–W–B(6)	99.8(4)	Fe–W–B(6)	54.0(3)
Fe–B(6)–W	67.3(4)	W–Fe–B(6)	58.8(3)	C(01)–W–B(6)	119.1(5)	C(02)–W–B(6)	158.8(5)
C(03)–Fe–B(6)	128.3(6)	C(04)–Fe–B(6)	117.1(7)	C(1)–W–C(40)	167.2(4)	C(1)–W–B(3)	152.2(5)
C(1)–W–C(20)	116.3(5)	Fe–Hb(6)–B(6)	96(1)	C(1)–Fe–B(6)	111.6(5)	W–C(01)–O(01)	163.2*
W–C(02)–O(02)	155.1*	Fe–C(03)–O(03)	163.1*	Fe–C(04)–O(04)	160.4*		

* Mean angle for disordered carbonyl ligand (see text).

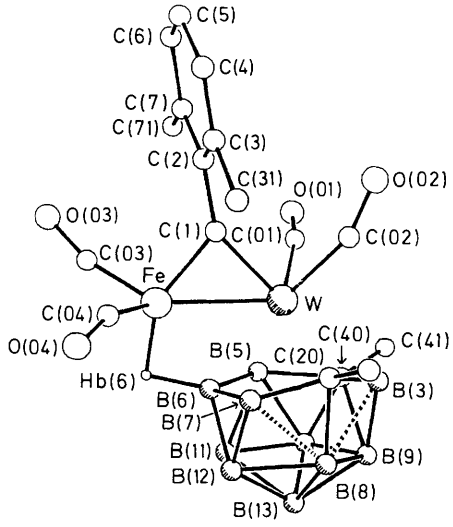

Figure 2. The structure of the anion of $[NEt_4][WFe(\mu\text{-}CC_6H_3Me_2\text{-}2,6)(CO)_4(\eta^6\text{-}C_2B_{10}H_{10}Me_2)]$ (**5**), showing the crystallographic numbering

attached to the boron atoms. In the $^{11}B\text{-}\{^1H\}$ n.m.r. spectra of the structurally related compounds $[NEt_4][MFe_2(\mu_3\text{-}CC_6H_4\text{-}Me\text{-}4)(\mu\text{-}\sigma\text{:}\sigma'\text{:}\eta^5\text{-}C_2B_9H_7Me_2)(CO)_8]$ (M = Mo or W) the corresponding peaks for the boron nuclei σ bonded to the iron atoms occur at δ 47.8 and 59.0 p.p.m. (Mo),[1] and 45.1 and 55.9 p.p.m. (W).[2g] The presence of the two B–Fe bonds in (**4**) introduces rigidity in the cage so that fluxional behaviour of the type discussed previously is not observed.

The corresponding reaction between complex (**1b**) and $[Fe_2(CO)_9]$ proceeds in a different manner, yielding as the only product a novel dimetal tetracarbonyl complex $[NEt_4][WFe(\mu\text{-}CC_6H_3Me_2\text{-}2,6)(CO)_4(\eta^6\text{-}C_2B_{10}H_{10}Me_2)]$ (**5**). Analytical and spectroscopic data are given in Tables 1 and 2. We have previously reported[2h] the synthesis of the pentacarbonyl compound $[NEt_4][WFe(\mu\text{-}CC_6H_3Me_2\text{-}2,6)(CO)_5(\eta^5\text{-}C_2B_9H_9Me_2)]$ from the reaction between $[NEt_4][W(\equiv CC_6H_3Me_2\text{-}2,6)(CO)_2(\eta^5\text{-}C_2B_9H_9Me_2)]$ and iron carbonyls. In this compound an *X*-ray diffraction study showed that the carbaborane group adopts a spectator role, with the C≡W bond present in the tungsten precursor ligating an $Fe(CO)_3$ group. The i.r. spectrum in the CO region shows five bands, whereas the spectrum of (**5**) has three carbonyl absorptions (Table 1). In order to resolve the structure of (**5**) an *X*-ray diffraction study was carried out. The results are summarised in Table 4, and the structure of the anion is shown in Figure 2.

The four CO ligands each showed positional disorder of the oxygen atoms between two alternative sites. Resolution of two such sites for the associated carbon atoms was not possible since high thermal motion was observed. The mean angles are: W–C(01)–O(01) 163.2, W–C(02)–O(02) 155.1, Fe–C(03)–O(03) 163.1, and Fe–C(04)–O(04) 160.4°. The most notable features in the structure are the presence of the relatively rare $Fe(CO)_2$ fragment, and the exopolyhedral bonding of the $C_2B_{10}H_{10}Me_2$ group so as to form a B–H→Fe bond. The boron [B(6)] involved in this linkage is the unique boron in the $\overline{CBCBBB}$ face, and is bonded only to other boron nuclei. The hydrogen atom [Hb(6)] was located and refined isotropically. Although the errors associated with connectivities to this hydrogen atom are large, the Fe–Hb(6) bond distance (1.7 Å) agrees well with the Ru–H (1.67 Å)[2b] and Mo–H (1.719 Å)[2c] distances in the molecules $[WRu(\mu\text{-}CC_6H_4Me\text{-}4)(CO)_3(\eta\text{-}C_5H_5)(\eta^5\text{-}C_2B_9H_9Me_2)]$ and $[WMo(\mu\text{-}CC_6H_4Me\text{-}4)(CO)_3(\eta^5\text{-}C_9H_7)(\eta^5\text{-}C_2B_9H_9Me_2)]$ (C_9H_7 = indenyl), both of which contain exopolyhedral B–H→M (M = Ru or Mo) bonds. The B(6)–Fe [2.20(1) Å] and B(6)–W [2.33(1) Å] distances in (**5**) are, however, significantly shorter and longer, respectively, than the corresponding B–W, B–Ru, or B–Mo distances in the aforementioned WRu and WMo species [B–Ru 2.400(7), B–W 2.248(8); and B–Mo 2.49 (2), B–W 2.26(2) Å, respectively]. This reflects the larger coordination face of the $\eta^6\text{-}C_2B_{10}H_{10}Me_2$ ligand in (**5**) *versus* the smaller $\eta^5\text{-}C_2B_9H_9Me_2$ fragment in the WRu and WMo compounds.

The non-planar character of the $\overline{CBCBBB}$ face of the ligand in (**5**) is well evidenced by the appreciable variations in the distances of the six atoms from the tungsten [W–C(20) 2.19(1), W–B(3) 2.46(2), W–C(40) 2.51(1), W–B(5) 2.35(1), W–B(6) 2.33(1), and W–B(7) 2.44(1) Å]. As found with (**1b**), the longest and shortest connectivities to the tungsten are associated with the two carbon atoms. Moreover, C(20), associated with the shortest separation, as expected is the cage vertex with lowest connectivity in the framework. Additionally, the long connectivities (represented in Figure 2 by dashed lines)

B(3) · · · B(8) [2.00(2)] and B(7) · · · B(8) [1.97(2) Å] involve the high-co-ordinate B(8) vertex, and result in two square faces sited about C(20). The high connectivity associated with B(8) is manifested in the long B(8)–B(9) and B(8)–B(12) distances of 1.87(3) and 1.89(3) Å, respectively. Moreover the low-co-ordinate atom C(20), as in (**1b**), displays relatively short distances to B(7) [1.56(2)] and B(3) [1.58(2) Å].

The plane defined by the xylyl ring is at an angle of 92.4° to the W$\overline{C(1)}$Fe ring. The $C_6H_3Me_2$-2,6 ring is also approximately orthogonal to the W$\overline{(\mu\text{-}C)}$Fe ring in the compound $[NEt_4][WFe(\mu\text{-}CC_6H_3Me\text{-}2,6)(CO)_5(\eta^5\text{-}C_2B_9H_9Me_2)]$.[2h] The metal–metal bond distance [2.512(2) Å] is very short, as expected for a W=Fe bond. Compound (**5**) is electronically unsaturated (32 valence electrons), as is $[NEt_4][WFe(\mu\text{-}CC_6H_3Me_2\text{-}2,6)(CO)_5(\eta^5\text{-}C_2B_9H_9Me_2)]$, but in the latter[2h] the W=Fe distance [2.600(1) Å] is longer than in (**5**). It is also instructive to compare the metal–metal distance in (**5**) with that in $[WFe\{\mu\text{-}C(C_6H_4Me\text{-}4)C(Me)C(Me)\}(CO)_5(\eta\text{-}C_5H_5)]$ [2.720(1) Å],[15] an electronically saturated (34 valence electron) complex having a W–Fe single bond. The W–C(1) distance [2.02(1) Å] is appreciably longer than that in $[NEt_4][WFe(\mu\text{-}CC_6H_3Me_2\text{-}2,6)(CO)_5(\eta^5\text{-}C_2B_9H_9Me_2)]$ [1.976(8) Å], but agrees well with the W–μ-C separation in the 32-valence electron species $[WFe(\mu\text{-}CC_6H_4Me\text{-}4)(CO)_5\{HB(pz)_3\}]$ [$HB(pz)_3$ = hydrotris(pyrazol-1-yl)borate] [2.025(1) Å][16] and $[WFe(\mu\text{-}CC_6H_4Me\text{-}4)(CO)_4(PBu^t{}_2H)(\eta\text{-}C_5H_5)]$ [2.018(5) Å].[17] Similar relationships hold for the Fe–μ-C distances. That in (**5**) [1.82(1) Å] is similar to those in $[WFe(\mu\text{-}CC_6H_4Me\text{-}4)(CO)_5\{HB(pz)_3\}]$ [1.826(6) Å][16] and $[WFe(\mu\text{-}CC_6H_4Me\text{-}4)(CO)_4(PBu^t{}_2H)(\eta\text{-}C_5H_5)]$ [1.850(4) Å],[17] but is perceptibly shorter than that in $[NEt_4][WFe(\mu\text{-}CC_6H_3Me_2\text{-}2,6)(CO)_5(\eta^5\text{-}C_2B_9H_9Me_2)]$ [1.891(5) Å].[2h]

As discussed earlier,[2h,11,16] the bonding within the W$\overline{(\mu\text{-}C)}$Fe ring in (**5**), and in the other related 32-valence electron dimetal species, is best understood in terms of a C≡W group acting as a four-electron donor to an $Fe(CO)_3$ fragment. This accounts for the short metal–metal bond, and the relative lengthening and shortening of the W–μ-C and Fe–μ-C distances, respectively, compared with those observed in 34-valence electron dimetal systems. In (**5**) the unprecedently short tungsten–iron distance is probably in part associated with the bridge bonding of the docosahedral carbaborane fragment, the presence of the B–H→Fe linkage forcing dissociation of a CO ligand from the iron centre. As is well known, $Fe(CO)_2$ groups are much less common than $Fe(CO)_3$ moieties in organoiron compounds.

Variable-temperature n.m.r. studies revealed that (**5**) underwent fluxional behaviour of the carbaborane cage system at ambient temperatures. Low-temperature-limiting ^1H and $^{13}C\text{-}\{^1H\}$ spectra, however, were observed at −40 °C (Table 2). The spectra are best measured on freshly prepared solutions, since some dissociation of complex (**5**) occurs affording (**1b**), and resonances due to the latter may be detected.

The ^1H n.m.r. spectrum (−40 °C) of (**5**) shows a diagnostic broad quartet resonance for the B–H→Fe group at δ −0.40 [J(BH) 84 Hz]. This signal is more deshielded than the resonances for the B–H→Ru (δ −11.48) and B–H→Mo (δ −7.98) groups, respectively, in the compounds $[WRu(\mu\text{-}CC_6H_4Me\text{-}4)(CO)_3(\eta\text{-}C_5H_5)(\eta^5\text{-}C_2B_9H_9Me_2)]$[2b] and $[WMo(\mu\text{-}CC_6H_4Me\text{-}4)(CO)_3(\eta^5\text{-}C_9H_7)(\eta^5\text{-}C_2B_9H_9Me_2)]$.[2c]

The ^1H n.m.r. spectrum (−40 °C) also shows four peaks in the methyl group region, corresponding to the presence of two non-equivalent cage CMe substituents, and two non-equivalent xylyl Me groups. The $^{13}C\text{-}\{^1H\}$ n.m.r. spectrum is in agreement, also displaying four resonances for the C*Me* and Me_2-2,6 groups. Moreover, the asymmetry of the structure is underlined by the appearance of six peaks for the C_6H_3 ring system. The CO resonances at δ 213.3 and 202.5 p.p.m. were readily assigned to WCO groups due to the presence of ^{183}W satellite peaks [J(WC) 130 and 153 Hz, respectively]. Unusually, the two resonances (δ 219.6 and 216.8 p.p.m.) for the $Fe(CO)_2$ fragment are more deshielded than those carbonyl groups ligating the tungsten.

The alkylidyne-carbon resonance for (**5**) is seen at δ 369.2 p.p.m. This chemical shift is in the range observed for other dimetal compounds wherein the C≡W fragment formally donates four electrons to a metal centre. The analogy with alkynes functioning as two- or four-electron donors in alkyne-metal complexes has been discussed elsewhere.[11]

The results described in this paper indicate that the salts (**1**) are promising reagents for the synthesis of compounds with heteronuclear metal–metal bonds. Moreover, the presence of the *nido*-docosahedral $\eta^6\text{-}C_2B_{10}H_{10}Me_2$ ligand introduces differences in reactivity patterns and properties of the products compared with analogous reactions involving salts of the anions $[W(\equiv CR)(CO)_2(\eta^5\text{-}C_2B_9H_9Me_2)]^-$ (R = alkyl or aryl).[2] It is to be anticipated that the larger and electronically different docosahedral fragment $C_2B_{10}H_{10}Me_2$ in the salts (**1**) will result in new discoveries in this area.

Experimental

Experiments were carried out using Schlenk-tube techniques, under a dry oxygen-free nitrogen atmosphere. Light petroleum refers to that fraction of b.p. 40—60 °C. Chromatography columns were of alumina (Brockman Activity II) or Florisil (100—200 mesh). The compounds $[AuCl(PPh_3)]$,[18] $[Rh(cod)(PPh_3)_2][PF_6]$,[19] and $Na_2[C_2B_{10}H_{10}Me_2]$[4b] were prepared by literature methods. The complexes $[W(\equiv CR)Cl(CO)_2L_2]$ (R = C_6H_4Me-4 or $C_6H_3Me_2$-2,6; L = pyridine or 4-methylpyridine) were obtained by the route reported for the CPh analogue.[20] Analytical and other data for the new compounds are given in Table 1. The instrumentation used for spectroscopic measurements has been reported previously.[2] The chemical shifts δ (p.p.m.) for the $^{11}B\text{-}\{^1H\}$ and $^{31}P\text{-}\{^1H\}$ n.m.r. data are positive to high frequency of $BF_3{\cdot}Et_2O$ (external) and 85% H_3PO_4 (external), respectively.

Synthesis of the Salts $[NEt_4][W(\equiv CR)(CO)_2(\eta^6\text{-}C_2B_{10}H_{10}Me_2)]$ (R = C_6H_4Me-4 *or* $C_6H_3Me_2$-2,6).—(*i*) The carbaborane $C_2B_{10}H_{10}Me_2$ (1.50 g, 8.71 mmol) and naphthalene (0.067 g, 0.52 mmol) were dissolved in thf (40 cm^3), and an excess of sodium metal (0.60 g) was added, and crushed to expose a fresh metal surface. The mixture was stirred for 2.5 h, and the dark green solution obtained was removed with a syringe and added to $[W(\equiv CC_6H_4Me\text{-}4)Cl(CO)_2(py)_2]$ (py = pyridine) (4.67 g, 8.71 mmol) dissolved in thf (25 cm^3). An additional 10 cm^3 of thf was used to wash the sodium residue, and the washings were added to the reaction mixture, which was stirred for another 3 h. After addition of $[NEt_4]Cl$ (2.9 g, 17.5 mmol), and further stirring (1 h), solvent was removed *in vacuo* affording a sticky residue. The latter was treated with CH_2Cl_2 (40 cm^3) and the resulting suspension was passed through a Celite pad (2 × 3 cm). Additional CH_2Cl_2 (3 × 20 cm^3) was used to wash the residue. Filtration through the Celite was repeated, and the solution obtained was combined with the first filtrate. The volume of solvent was reduced *in vacuo* to *ca.* 20 cm^3, and the solution was chromatographed at −40 °C on alumina. Elution with CH_2Cl_2 removed a broad bright yellow band. Removal of solvent *in vacuo* gave a sticky yellow residue, which after washing with Et_2O (4 × 30 cm^3) afforded yellow *microcrystals* of $[NEt_4][W(\equiv CC_6H_4Me\text{-}4)(CO)_2(\eta^6\text{-}C_2B_{10}H_{10}Me_2)]$ (**1a**) (4.05 g).

(*ii*) Similarly, a thf (15 cm^3) solution of $[W(\equiv CC_6H_3Me_2$-

2,6)Cl(CO)$_2$(4Me-py)$_2$] (4Me-py = 4-methylpyridine) (0.67 g, 1.16 mmol) was treated with a dark green solution of $Na_2[C_2B_{10}H_{10}Me_2]$ (1.16 mmol) in the same solvent (5 cm^3). After 3 h, [NEt$_4$]Cl (0.40 g, 2.4 mmol) was added, and the mixture was stirred for an additional 1 h. Solvent was removed *in vacuo*. The residue was treated with CH_2Cl_2 (25 cm^3) and the resulting suspension was filtered through a Celite pad (2 × 3 cm). The residue was further extracted with CH_2Cl_2 (3 × 15 cm^3) and the extracts, after filtration through the Celite, were combined with the initial filtrate. Solvent was reduced in volume *in vacuo* to *ca.* 20 cm^3, and the solution was chromatographed at −40 °C on alumina. Elution with CH_2Cl_2 afforded a yellow eluate. The latter was concentrated to *ca.* 15 cm^3, and light petroleum (70 cm^3) was added, affording yellow *microcrystals* of $[NEt_4][W(\equiv CC_6H_3Me_2\text{-}2,6)(CO)_2(\eta^6\text{-}C_2B_{10}H_{10}Me_2)]$ (**1b**) (0.54 g), after removal of solvent with a syringe.

Reactions of the Salts $[NEt_4][W(\equiv CR)(CO)_2(\eta^6\text{-}C_2B_{10}H_{10}Me_2)]$ (R = C_6H_4Me-4 *or* $C_6H_3Me_2$-2,6).—(*i*) A thf (15 cm^3) solution of complex (**1a**) (0.20 g, 0.32 mmol) was treated with [AuCl(PPh$_3$)] (0.16 g, 0.32 mmol) and KPF_6 (0.07 g, 0.40 mmol), and the mixture was stirred for 2 h. The solution was reduced in volume *in vacuo* to *ca.* 5 cm^3, and chromatographed on Florisil at room temperature. Elution with thf removed a yellow eluate, from which solvent was removed *in vacuo*. The residue was dissolved in CH_2Cl_2 (3 cm^3), and light petroleum (100 cm^3) was added, giving yellow *microcrystals* of $[WAu(\mu\text{-}CC_6H_4Me\text{-}4)(CO)_2(PPh_3)(\eta^6\text{-}C_2B_{10}H_{10}Me_2)]$ (**2a**) (0.25 g), after removal of solvent with a syringe. Phosphorus-31 n.m.r.: δ 52.3 p.p.m. (in CD_2Cl_2–CH_2Cl_2).

(*ii*) In a similar manner, [AuCl(PPh$_3$)] (0.13 g, 0.27 mmol) and KPF_6 (0.07 g, 0.40 mmol) were added to complex (**1b**) (0.18 g, 0.27 mmol) in thf (15 cm^3), and the mixture was stirred for 24 h. Solvent was removed *in vacuo*, and the residue was dissolved in thf–Et$_2$O (5 cm^3, 4:1) and chromatographed on Florisil. Elution with the same solvent mixture gave a bright yellow eluate. Removal of solvent *in vacuo*, followed by washing the residue with light petroleum (3 × 10 cm^3), afforded yellow *microcrystals* of $[WAu(\mu\text{-}CC_6H_3Me_2\text{-}2,6)(CO)_2(PPh_3)(\eta^6\text{-}C_2B_{10}H_{10}Me_2)]$ (**2b**) (0.15 g). Analytically pure samples can be obtained by recrystallisation from acetone. Phosphorus-31 n.m.r.: δ 49.3 p.p.m. (in CD_2Cl_2–CH_2Cl_2).

(*iii*) Treatment of complex (**1a**) (0.20 g, 0.31 mmol) in thf (15 cm^3) with $[Rh(cod)(PPh_3)_2][PF_6]$ (0.27 g, 0.31 mmol) resulted in an immediate colour change from bright yellow to dark brown. After stirring the mixture for 2 h, solvent was removed *in vacuo*. The residue was dissolved in CH_2Cl_2 (8 cm^3), and light petroleum (*ca.* 120 cm^3) was added. After *ca.* 10 min a dark brown product precipitated, from which a red solution was decanted. After pumping *in vacuo* the brown precipitate was dissolved in Et$_2$O–CH_2Cl_2 (15 cm^3, 1:1), and chromatographed on alumina. Elution with the same solvent mixture afforded a brown eluate, which after removal of solvent *in vacuo* gave a brown solid. The latter was recrystallised from CH_2Cl_2 (4 cm^3) and light petroleum (60 cm^3) to give brown *microcrystals* of $[WRh(\mu\text{-}CC_6H_4Me\text{-}4)(CO)_2(PPh_3)_2(\eta^6\text{-}C_2B_{10}H_{10}Me_2)]$ (**3a**) (0.30 g). Boron-11 n.m.r.: δ 21.8 [1 B, B(μ-H)Rh] and −7.1 p.p.m. (vbr, 9 B) (in CD_2Cl_2–CH_2Cl_2 at −60 °C). Phosphorus-31 n.m.r.: major isomer, δ 52.2 [d of d, *J*(PP) 29, *J*(RhP) 162] and 38.5 p.p.m. [d of d, *J*(PP) 28, *J*(RhP) 148 Hz]; minor isomer, δ 41.3 [d of d, *J*(PP) 26, *J*(RhP) 172] and 27.8 p.p.m. [d of d, *J*(PP) 25, *J*(RhP) 146 Hz] (in CD_2Cl_2–CH_2Cl_2, at −80 °C).

(*iv*) A thf (15 cm^3) solution of complex (**1b**) (0.17 g, 0.27 mmol) was treated with $[Rh(cod)(PPh_3)_2][PF_6]$ (0.24 g, 0.27 mmol), and the mixture was stirred for 24 h. Solvent was removed *in vacuo* and the residue was dissolved in Et$_2$O–CH_2Cl_2 (5 cm^3, 1:1) and chromatographed on Florisil. Elution with the same solvent mixture removed an orange band containing decomposed material, and this was discarded. Further elution gave a green fraction. This was collected, solvent was removed *in vacuo*, and the residue was washed (4 × 15 cm^3) with light petroleum–CH_2Cl_2 (6:1) giving, after drying *in vacuo*, green *microcrystals* of $[WRh(\mu\text{-}CC_6H_3Me_2\text{-}2,6)(CO)_2(PPh_3)_2(\eta^6\text{-}C_2B_{10}H_{10}Me_2)]$ (**3b**) (0.25 g). Phosphorus-31 n.m.r.: δ 33.2 [d of d, *J*(PP) 32, *J*(RhP) 169] and 26.5 p.p.m. [d of d, *J*(PP) 32, *J*(RhP) 146 Hz] (in CD_2Cl_2–CH_2Cl_2, at −80 °C).

(*v*) Treatment of a thf (20 cm^3) solution of complex (**1a**) (0.20 g, 0.31 mmol) with $[Fe_2(CO)_9]$ (0.45 g, 1.24 mmol) afforded, after stirring for *ca.* 18 h and removal of solvent *in vacuo*, a dark green residue. The latter was dissolved in CH_2Cl_2 (15 cm^3) and chromatographed on alumina at −40 °C. Elution with the same solvent removed a broad green band. The eluate was concentrated *in vacuo* to *ca.* 20 cm^3, and light petroleum (80 cm^3) was layered upon the CH_2Cl_2 solution without mixing. After *ca.* 15 h green *crystals* of $[NEt_4][WFe_2(\mu_3\text{-}CC_6H_4Me\text{-}4)(\mu\text{-}\sigma:\sigma':\eta^6\text{-}C_2B_{10}H_8Me_2)(CO)_8]$ (**4**) (0.20 g) were recovered, after decanting the supernatant solution. Boron-11 n.m.r.: δ 58.8, 47.3 (2 B, BFe), −1.3 (2B), −3.4 (1B), −4.8 (2B), −8.8 (1B), and −13.2 p.p.m. (2B) (in CD_2Cl_2–CH_2Cl_2).

(*vi*) Addition of $[Fe_2(CO)_9]$ (0.83 g, 2.27 mmol) to a thf (20 cm^3) solution of complex (**1b**) (0.50 g, 0.76 mmol), followed by stirring for 2 h, and removal of solvent *in vacuo*, gave a dark residue. The latter was washed with Et$_2$O (5 × 20

Table 5. Atomic positional parameters (fractional co-ordinates, × 10^4) for complex (**1b**), with estimated standard deviations (e.s.d.s) in parentheses

Atom	*x*	*y*	*z*
W	2 638(1)	1 038(1)	1 151(1)
N	8 501(7)	3 473(5)	1 419(5)
C(1N)	7 603(10)	3 928(8)	1 524(7)
C(2N)	6 878(14)	3 628(10)	1 981(8)
C(3N)	9 091(10)	3 862(7)	974(6)
C(4N)	10 065(11)	3 548(9)	804(7)
C(5N)	9 104(12)	3 363(9)	1 948(7)
C(6N)	9 416(16)	4 017(11)	2 243(9)
C(7N)	8 262(17)	2 733(11)	1 255(8)
C(8N)	7 641(16)	2 663(14)	755(10)
C(1)	2 050(8)	766(6)	473(4)
C(2)	1 566(7)	512(6)	−25(4)
C(3)	747(8)	880(6)	−277(5)
C(4)	298(8)	604(7)	−754(5)
C(5)	635(10)	9(8)	−1 000(6)
C(6)	1 428(11)	−345(7)	−764(5)
C(7)	1 906(9)	−120(6)	−279(5)
C(31)	355(10)	1 526(8)	−10(6)
C(71)	2 759(10)	−522(8)	−6(6)
C(01)	2 096(10)	139(7)	1 433(6)
O(01)	1 814(9)	−381(6)	1 587(5)
C(02)	1 336(10)	1 488(7)	1 357(5)
O(02)	602(8)	1 759(8)	1 456(5)
C(20)	3 250(10)	2 122(6)	1 215(5)
C(40)	3 712(10)	1 118(7)	2 054(5)
C(21)	2 701(14)	2 795(9)	1 080(8)
C(41)	3 196(14)	828(8)	2 583(6)
B(7)	3 948(11)	1 787(8)	770(7)
B(3)	3 298(11)	1 903(8)	1 849(7)
B(5)	4 148(10)	551(6)	1 525(6)
B(6)	4 381(11)	916(8)	833(6)
B(12)	5 201(12)	1 619(8)	964(8)
B(8)	4 525(12)	2 240(8)	1 453(9)
B(11)	5 363(11)	827(7)	1 345(7)
B(10)	4 956(13)	957(8)	2 041(8)
B(9)	4 526(13)	1 769(9)	2 154(8)
B(13)	5 499(12)	1 664(8)	1 682(8)

Table 6. Atomic positional parameters (fractional co-ordinates, $\times 10^4$) for complex (**5**), with e.s.d.s in parentheses

Atom	*x*	*y*	*z*	Atom	*x*	*y*	*z*
W	2 004(1)	1 428(1)	1 596(1)	B(8)	4 668(13)	1 506(13)	2 176(11)
Fe	1 484(1)	719(1)	2 835(1)	B(9)	4 719(12)	1 114(10)	1 122(11)
O(01)	401(14)	688(12)	25(11)	B(10)	4 200(10)	111(9)	1 064(9)
O(01A)	447(14)	1 135(12)	22(11)	B(11)	3 954(13)	−253(9)	2 041(10)
O(02)	832(14)	3 076(11)	966(10)	B(12)	4 292(12)	535(11)	2 737(9)
O(02A)	1 543(13)	3 397(10)	1 198(9)	B(13)	5 072(13)	422(12)	1 946(13)
O(03)	−470(16)	−273(12)	3 000(12)	N	2 805(10)	8 605(8)	5 263(6)
O(03A)	−44(16)	−415(12)	3 262(12)	C(1N)	1 961(21)	8 581(20)	4 651(16)
O(04)	2 003(15)	1 255(11)	4 579(11)	C(2N)	979(26)	8 183(20)	4 937(19)
O(04A)	1 373(16)	1 378(13)	4 425(11)	C(3N)	3 870(17)	8 995(14)	4 945(12)
C(20)	3 478(9)	2 097(8)	2 087(8)	C(4N)	4 213(19)	8 630(18)	4 151(15)
C(21)	3 615(14)	3 019(10)	2 381(14)	C(5N)	3 255(17)	7 574(14)	5 364(12)
C(40)	3 394(9)	941(7)	766(7)	C(6N)	4 355(18)	7 369(14)	5 829(14)
C(41)	3 098(11)	984(11)	−158(8)	C(7N)	2 861(17)	8 847(14)	6 132(13)
C(01)	979(9)	1 099(10)	611(7)	C(8N)	2 564(21)	9 800(17)	6 147(16)
C(02)	1 494(14)	2 578(10)	1 262(8)	C(1NA)	1 645(20)	9 022(16)	4 718(15)
C(03)	434(12)	67(8)	2 998(8)	C(2NA)	726(26)	9 323(22)	5 186(20)
C(04)	1 607(16)	1 052(9)	3 845(8)	C(3NA)	3 020(22)	9 333(19)	5 926(16)
C(1)	758(8)	1 553(7)	2 227(6)	C(4NA)	3 348(25)	192(21)	5 550(19)
C(2)	−242(8)	1 987(9)	2 317(6)	C(5NA)	3 406(23)	8 525(21)	4 677(18)
C(3)	−224(10)	2 742(8)	2 760(7)	C(6NA)	4 489(35)	8 012(29)	5 253(26)
C(31)	819(10)	3 097(8)	3 172(7)	C(7NA)	2 328(31)	7 952(26)	5 797(23)
C(4)	−1 148(11)	3 138(9)	2 833(9)	C(8NA)	1 852(26)	7 175(21)	5 189(19)
C(5)	−2 136(12)	2 800(11)	2 471(10)	Hb(6)	2 454(83)	−6(72)	2 871(65)
C(6)	−2 176(10)	2 083(12)	2 048(9)	Hb(5)	2 147	−292	955
C(7)	−1 217(9)	1 630(9)	1 944(6)	Hb(9)	5 212	1 368	653
C(71)	−1 297(11)	808(13)	1 441(9)	Hb(7)	3 252	1 493	3 474
B(3)	3 701(13)	1 915(10)	1 194(12)	Hb(10)	4 349	−445	655
B(5)	2 863(10)	160(7)	1 322(7)	Hb(11)	4 131	−850	2 280
B(6)	2 968(10)	374(8)	2 363(8)	Hb(12)	4 707	525	3 355
B(7)	3 421(9)	1 414(10)	2 759(8)				

cm^3), and the dark green solid was dissolved in CH_2Cl_2 (10 cm^3). Light petroleum (50 cm^3) was carefully layered on top of the CH_2Cl_2 without undue mixing. After *ca.* 15 h dark green rod-like *crystals* of $[NEt_4][WFe(\mu\text{-}CC_6H_3Me_2\text{-}2,6)(CO)_4(\eta^6\text{-}C_2B_{10}H_{10}Me_2)]$ (**5**) (0.24 g) were recovered, after decantation of solvent. Also formed were a few bright yellow crystals of (**1b**), which result from the decomposition of (**5**). These yellow crystals are easily removed mechanically. It is essential that the crystallisation of (**5**) be done in a large bore (*ca.* 4 cm) Schlenk tube to ensure good diffusion between the two solvents. A second crop of *crystals* of (**5**) (0.18 g) was recovered from the decanted supernatant liquid by addition of more light petroleum (50 cm^3). Boron-11 n.m.r.: δ 23.0 [1 B, B(μ-H)Fe], −0.4, −5.7, −9.5, −11.0, and −19.2 p.p.m. (9 B) (in CD_2Cl_2–CH_2Cl_2, at −40 °C).

Crystal Structure Determinations.—Crystals of complex (**1b**) were obtained by layering light petroleum (5 cm^3) on to CH_2Cl_2 (1 cm^3) solutions without solvent mixing. After several days at room temperature bright yellow crystals of (**1b**) were collected. In a similar manner dark green crystals were obtained by layering light petroleum (50 cm^3) on to a CH_2Cl_2 (10 cm^3) solution of (**5**). Crystals chosen for study [(**1b**), *ca.* 0.30 × 0.56 × 0.075; (**5**), *ca.* 0.50 × 0.50 × 0.50 mm] were sealed under nitrogen in Lindemann tubes. For (**1b**) diffracted intensities were collected (θ–2θ scans) at 293 K in the range $3 \leqslant 2\theta \leqslant 50°$. Of the 5 979 unique intensities measured, 3 052 had $F \geqslant 3\sigma(F)$, and only these were used in the solution and refinement. For (**5**), 6 488 unique data were collected (θ–2θ scans) at 200 K in the range $2\theta \leqslant 50°$. Of these unique intensities, 4 139 had $F \geqslant 2\sigma(F)$, and only these were used in the structural solution and refinement.

Data were collected on a Nicolet *P3m* four-circle diffractometer, and were corrected for Lorentz, polarisation, and *X*-ray absorption effects. The latter was by a numerical method for (**1b**) (developed crystal faces ⟨100⟩, ⟨010⟩, ⟨001⟩), and by a method based on azimuthal scan data for (**5**).[21]

Crystal data for (**1b**). $C_{23}H_{45}B_{10}NO_2W$, $M = 659.57$, orthorhombic, $a = 13.380(3)$, $b = 19.381(6)$, $c = 23.357(7)$ Å, $U = 6\,057(2)$ Å^3, $Z = 8$, $D_c = 1.45$ g cm^{-3}, $F(000)$ 2 640, space group *Pbca*, Mo-K_α *X*-radiation (graphite monochromator), $\bar{\lambda} = 0.710\,69$ Å, μ(Mo-K_α) = 39.2 cm^{-1}.

Crystal data for (**5**). $C_{25}H_{45}B_{10}FeNO_4W$, $M = 771.45$, monoclinic, $a = 12.637(2)$, $b = 15.782(2)$, $c = 16.609(2)$ Å, $\beta = 98.39(1)°$, $U = 3\,277(1)$ Å^3, $Z = 4$, $D_c = 1.57$ g cm^{-3}, $F(000) = 1\,536$, space group $P2_1/c$ (no. 14), Mo-K_α *X*-radiation (graphite monochromator), $\bar{\lambda} = 0.710\,69$ Å, μ(Mo-K_α) = 40.56 cm^{-1}.

Structure solutions and refinements. The structures were solved by conventional heavy-atom methods on a Digital μ-Vax computer using the SHELXPLUS package. All non-hydrogen atoms were located from Fourier difference synthesis, and refined with anisotropic thermal parameters. The aryl hydrogen atoms were incorporated at calculated positions (C–H 0.96 Å) with tied isotropic thermal parameters (*ca.* 1.2 $U_{equiv.}$ of the parent carbon atoms). The hydrogen atoms in the carbaborane cage of (**1b**) were located and refined with a common isotropic thermal parameter (*ca.* 1.2 $U_{equiv.}$ of the parent boron atom). For complex (**5**) the hydrogens attached to boron and located from difference density maps were added to the final calculations as fixed spherical atoms, except Hb(6) which was successfully refined isotropically.

The four CO groups in (**5**) showed disorder, as discussed earlier. In addition the NEt_4^+ cation was disordered with the C atoms of the Et groups showing alternative sites (50% occupancy) about the ordered N atoms. A weighting scheme of

the form $w^{-1} = [\sigma^2(F_o) + g|F_o|^2]$ gave a satisfactory analysis of variance with $g = 0.003\,75$ for (**1b**) and 0.000 50 for (**5**). The final electron-density difference synthesis showed no peaks $\geqslant \pm 1.5$ e Å^{-3}. Atomic scattering factors, with corrections for anomalous dispersion included in the programs,[21] were from ref. 22. Refinement converged at R 0.046 (R' 0.051) for (**1b**), and R 0.058 (R' 0.052) for (**5**). Atomic co-ordinates for (**1b**) and (**5**) are listed in Tables 5 and 6, respectively.

Additional material available from the Cambridge Crystallographic Data Centre comprises H-atom co-ordinates, thermal parameters, and remaining bond lengths and angles.

Acknowledgements

We thank the USAF Office of Scientific Research (Grant 86-0125) for partial support.

References

1 Part 86, D. D. Devore, C. Emmerich, J. A. K. Howard, and F. G. A. Stone, *J. Chem. Soc., Dalton Trans.*, 1989, 797.
2 (*a*) M. Green, J. A. K. Howard, A. P. James, C. M. Nunn, and F. G. A. Stone, *J. Chem. Soc., Dalton Trans.*, 1987, 61; (*b*) M. Green, J. A. K. Howard, A. N. de M. Jelfs, O. Johnson, and F. G. A. Stone, *ibid.*, p. 73; (*c*) M. Green, J. A. K. Howard, A. P. James, A. N. de M. Jelfs, C. M. Nunn, and F. G. A. Stone, *ibid.*, p. 81; (*d*) J. A. K. Howard, A. P. James, A. N. de M. Jelfs, C. M. Nunn, and F. G. A. Stone, *ibid.*, p. 1221; (*e*) M. L. Attfield, J. A. K. Howard, A. N. de M. Jelfs, C. M. Nunn, and F. G. A. Stone, *ibid.*, p. 2219; (*f*) F-E. Baumann, J. A. K. Howard, O. Johnson, and F. G. A. Stone, *ibid.*, p. 2661; (*g*) F-E. Baumann, J. A. K. Howard, O. Johnson, and F. G. A. Stone, *ibid.*, p. 2917; (*h*) F-E. Baumann, J. A. K. Howard, R. J. Musgrove, P. Sherwood, and F. G. A. Stone, *ibid.*, 1988, 1879, 1891; (*i*) D. D. Devore, J. A. K. Howard, J. C. Jeffery, M. U. Pilotti, and F. G. A. Stone, *ibid.*, 1989, 303.
3 F. G. A. Stone, *Pure Appl. Chem.*, 1986, **58**, 529, *ACS Symp. Ser.*, 1983, **211**, 383.
4 (*a*) K. P. Callahan and M. F. Hawthorne, *Adv. Organomet. Chem.*, 1976, **14**, 145; (*b*) D. F. Dustin, G. B. Dunks, and M. F. Hawthorne, *J. Am. Chem. Soc.*, 1973, **95**, 1109; (*c*) W. J. Evans, G. B. Dunks, and M. F. Hawthorne, *ibid.*, p. 4565.
5 D. D. Devore, S. J. B. Henderson, J. A. K. Howard, and F. G. A. Stone, *J. Organomet. Chem.*, 1988, **358**, C6.
6 (*a*) C. G. Salentine and M. F. Hawthorne, *J. Am. Chem. Soc.*, 1975, **97**, 426; *Inorg. Chem.*, 1976, **15**, 2872; (*b*) F. Y. Lo, C. E. Strouse, K. P. Callahan, C. B. Knobler, and M. F. Hawthorne, *J. Am. Chem. Soc.*, 1975, **97**, 428; (*c*) M. R. Churchill and B. G. DeBoer, *Inorg. Chem.*, 1974, **13**, 1411; (*d*) J. D. Hewes, C. B. Knobler, and M. F. Hawthorne, *J. Chem. Soc., Chem. Commun.*, 1981, 206.
7 N. W. Alcock, J. G. Taylor, and M. G. H. Wallbridge, *J. Chem. Soc., Dalton Trans.*, 1987, 1805.
8 R. N. Grimes, in 'Comprehensive Organometallic Chemistry,' eds. G. Wilkinson, F. G. A. Stone, and E. W. Abel, Pergamon, Oxford, 1982, vol. 1, section 5.5.
9 O. Johnson, J. A. K. Howard, M. Kapan, and G. M. Reisner, *J. Chem. Soc., Dalton Trans.*, 1988, 2903.
10 J. A. Abad, L. W. Bateman, J. C. Jeffery, K. A. Mead, H. Razay, F. G. A. Stone, and P. Woodward, *J. Chem. Soc., Dalton Trans.*, 1983, 2075.
11 S. J. Dossett, A. F. Hill, J. C. Jeffery, F. Marken, P. Sherwood, and F. G. A. Stone, *J. Chem. Soc., Dalton Trans.*, 1988, 2453.
12 F-E. Baumann, J. A. K. Howard, R. J. Musgrove, P. Sherwood, M. A. Ruiz, and F. G. A. Stone, *J. Chem. Soc., Chem. Commun.*, 1987, 1881.
13 J. A. Abad, E. Delgado, M. E. Garcia, M. J. Gross-Ophoff, I. J. Hart, J. C. Jeffery, M. S. Simmons, and F. G. A. Stone, *J. Chem. Soc., Dalton Trans.*, 1987, 41.
14 J. A. K. Howard and N. Sanders, unpublished work.
15 J. C. Jeffery, K. A. Mead, H. Razay, F. G. A. Stone, M. J. Went, and P. Woodward, *J. Chem. Soc., Dalton Trans.*, 1984, 1383.
16 M. Green, J. A. K. Howard, A. P. James, A. N. de M. Jelfs, C. M. Nunn, and F. G. A. Stone, *J. Chem. Soc., Dalton Trans.*, 1986, 1697.
17 M. Boual and J. C. Jeffery, unpublished work.
18 F. G. Mann, A. F. Wells, and D. Purdie, *J. Chem. Soc.*, 1937, 1828.
19 R. R. Schrock and J. A. Osborn, *J. Am. Chem. Soc.*, 1971, **93**, 2397.
20 G. A. McDermott, A. M. Dorries, and A. Mayr, *Organometallics*, 1987, **6**, 925.
21 G. M. Sheldrick, SHELXTL programs for use with the Nicolet *X*-ray system, Revision 5.1, 1986.
22 'International Tables for *X*-Ray Crystallography,' Kynoch Press, Birmingham, 1974, vol. 4.

Received 14*th June* 1988; *Paper* 8/02357C